PERGAMON

International Journal of Heat and Mass Transfer 45 (2002) 4967–4981

International Journal of HEAT and MASS TRANSFER

www.elsevier.com/locate/ijhmt

Experimental determination of the interfacial heat transfer during cooling and solidification of molten metal droplets impacting on a metallic substrate: effect of roughness and superheat

G.-X. Wang [a,*], E.F. Matthys [b]

[a] Department of Mechanical Engineering, The University of Akron, Akron, OH 44325-3903, USA

[b] Department of Mechanical and Environmental Engineering, University of California, Santa Barbara, CA 93106, USA

Received 21 March 2002; received in revised form 22 May 2002

Abstract

The interfacial heat transfer between a solidifying molten metal and a metallic substrate is critical in many processes such as strip casting and spray deposition. As the molten metal cools down and solidifies, the interface undergoes a change from the initial liquid/solid contact to a solid/solid contact, leading to very dynamic variations in the rate of interfacial heat transfer. This article presents the results of an experimental study of the contact heat transfer when molten nickel or copper droplets are dropped on an inclined metallic substrate. The interfacial heat transfer coefficient, h, between the melt and the substrate is evaluated by matching model calculations with the top splat surface temperature history measured by a fast-response pyrometer. The results suggest that a high value of the interfacial heat transfer coefficient h (10^4 to 3×10^5 W/m^2 K) is achieved when the molten splat is in contact with the substrate, followed by a smaller value ($<10^4$ W/m^2 K) during the later stages of solidification and the solid cooling phase. A parametric study was performed to investigate the effect on h of the metal/substrate materials combination, the melt superheat, and the substrate surface roughness, and some of the results are also presented.

© 2002 Elsevier Science Ltd. All rights reserved.

1. Introduction

Interfacial heat transfer between a solidifying molten metal and a colder substrate is a central issue in many materials processes involving solidification, such as mold casting, strip casting, and spray deposition. It affects the selection of phases, the crystalline nucleation, and the subsequent solidification process, and controls the microstructure development of the solidified products. As the molten metal cools down and solidifies, the interface undergoes a change from an initial liquid/solid contact to a solid/solid contact, leading to a strong dynamic variation in the rate of interfacial heat transfer. When molten metal is first put in contact with a colder substrate, a contact is formed between the molten metal and the substrate only at the asperities protruding from the surface due to the effect of the surface tension of the liquid metal [1]. This non-perfect contact results in a thermal resistance between the metal and the substrate. When the molten metal cools down, crystalline phases nucleate first on the contact points and then quickly spread to form a solid shell over the substrate. There are then numerous pores and gaps existing at the interface. As the liquid metal further solidifies, a contraction of the solid layer due to thermal stress may further enlarge the gaps at the interface and thus may result in a larger thermal resistance. A macroscopic gap may eventually develop between the cast metal and the substrate, dominating the thermal resistance at the interface.

Much work has been conducted in the literature attempting to understand and quantify this interfacial thermal contact resistance. Most of the earlier work,

* Corresponding author.

E-mail address: gwang@uakron.edu (G.-X. Wang).

0017-9310/02/$ - see front matter © 2002 Elsevier Science Ltd. All rights reserved.

PII: S0017-9310(02)00199-0

Nomenclature

b	thickness of the splat (μm)
C_1, C_2	constants in Eqs. (5) and (6)
C_p	specific heat (J/kg K)
h	interfacial heat transfer coefficient (W/m^2 K)
h_0	interfacial heat transfer coefficient during melt spreading (W/m^2 K)
h_1	interfacial heat transfer coefficient in the earlier stages of splat cooling and solid formation (W/m^2 K)
h_2	interfacial heat transfer coefficient during solidification or later stages of cooling (W/m^2 K)
h_3	interfacial heat transfer coefficient after solidification (W/m^2 K)
h_∞	convective heat transfer coefficient between the splat and the gas in the chamber (W/m^2 K)
H	height of droplet free fall (mm)
K	thermal conductivity (W/m K)
L	latent heat of solidification (J/kg)
n	exponent in Eqs. (5) and (6)
q	heat flux (W/m^2)
R_a	arithmetic average roughness of the substrate surface (μm)
t	time (ms or s)
t_1	transition time from h_0 to h_1 (ms)
t_2	transition time from h_1 to h_2 (ms)
t_3	transition time from h_2 to h_3 (ms)
t_N	calculated nucleation time (ms)
T	temperature (K)
T_S	initial substrate temperature (K)
T_M	equilibrium melting temperature (K)
T_{sb}	average temperature at the splat bottom surface (K)
T_{st}	temperature at the splat top surface (K)
T_{ss}	average temperature of the substrate surface (K)
T_p	temperature of the superheated melt upon impact (K)
ΔT_p	melt superheat upon impact, $T_p - T_M$ (K)
T_∞	gas temperature in the chamber (K)
V_i	interface velocity (m/s)
y	coordinate normal to the substrate (m)

Greek symbols

ε	average emissivity of the splat top surface
θ	substrate inclination angle
ρ	density

Subscripts

L	liquid
S	solid
i	interface
j	stands for substrate, solid, and melt, Eq. (1)

however, focused on the formation and development of the air-gap between casting metal and mold for systems with large dimensions such as conventional mold casting [2,3]. Recently, more attention was paid to the interfacial heat transfer during the early stages of melt cooling and solidification process, when an intimate contact exists between the solidifying metal and the substrate surface [4–8]. The heat transfer due to an intimate contact at the early stage of the process is important because it may ultimately determine the mechanical properties of the material. This is true, in particular, for those processes such as strip casting and spray deposition in which a thin layer of molten metal is put in contact with a colder substrate. In these processes, the melt cooling rate and the solidification rate are controlled by the interfacial heat transfer conditions between the casting and the substrate [9–11].

To present the experimental data, a majority of researchers in the field have used an "interfacial heat transfer coefficient" (usually denoted by "h") instead of the conventional thermal conductance or thermal resistance. Most of the early studies provided average values of such an interfacial heat transfer coefficient over an unspecified but long time period covering initial melt cooling, solidification, and solid phase cooling. Some of these results can be found in a review by the present authors [12].

The dynamic behavior of the interfacial heat transfer between a solidifying molten metal and a substrate have been also investigated recently by several authors using low melting point metals such as tin, lead, and zinc. Using measured temperature data, the interfacial heat transfer coefficient can be estimated as a function of time by solving an inverse heat transfer problem with the interfacial heat transfer coefficient as the free parameter. For example, we have estimated the dynamic variation of the interfacial heat transfer by using two thermocouples buried in a solidifying tin melt on a copper substrate [5]. Loulou et al. [6] and Wang and Qiu [7], on the other hand, have used semi-intrinsic thermocouples buried in the substrate. These studies have shown a strong dynamic variation of the interfacial heat transfer coefficient as the molten metal cools down and solidifies. Loulou et al. [6] have also studied the effect of processing conditions such as the melt super heat, surface roughness, and also the cast material used.

Many engineering materials, however, have much higher melting points than that of tin and zinc, which

may lead to a very different thermal contact condition at the interface. To quantify the interfacial heat transfer of high-melting point materials, the present authors have developed a splat cooling experimental method that is usable for metals such as copper and nickel. In the splat cooling experiment, a molten metal droplet is levitated electromagnetically and then dropped onto a metallic substrate to form a thin liquid splat, which is solidified quickly into a solid splat. The splat surface temperature is measured by an IR pyrometer. Using the measured temperature data, the interfacial heat transfer coefficient can be estimated by solving the inverse heat transfer problem. The early results for nickel splats [8] were obtained by using a two-color pyrometer with a relatively slow response time (about 25 ms). These results are valid only for the later cooling time period, after the splat is solidified. Later on, we used a single-color pyrometer with a much faster response time (about 1.5 ms) for copper splats [13]. In the present article, we report on a systematic study of the interfacial heat transfer during the melt cooling and the early stages of solidification for molten nickel or copper droplets quenched on various substrates under different surface conditions.

First we will give a brief overview of our experimental system. A discussion of the determination of the surface emissivity of the solidifying splats is then presented, because the surface emissivity affects the accuracy of the measured temperature data. Section 3 presents the mathematical model for splat cooling and the temperature matching method used to estimate the interfacial heat transfer coefficient. The main results are then presented in Section 4, with emphasis on the effect of the melt superheat and surface roughness on the interfacial heat transfer coefficient.

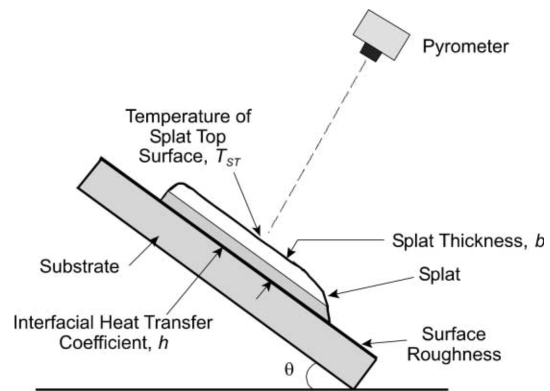

Fig. 1. A schematic diagram of the experimental setup.

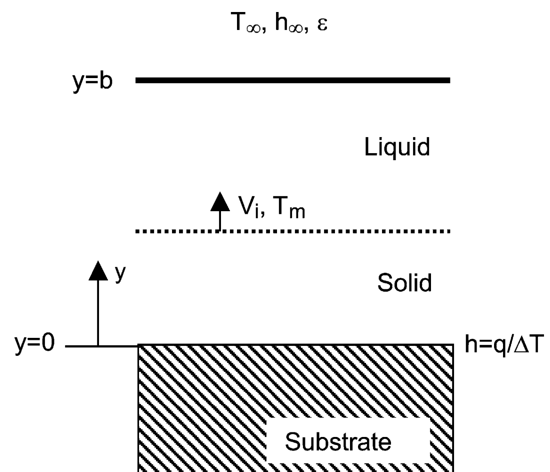

Fig. 2. One-dimensional heat transfer and solidification model for splat cooling.

2. Experimental system and temperature measurements

A detailed description of the experimental system has been given elsewhere [13,14], and only a brief summary is presented here. The experimental system was designed to provide a configuration that can be modeled as a one-dimensional heat transfer and solidification problem so that an inverse method can be easily used. This is accomplished by dropping a molten metallic droplet onto an inclined metallic surface to form quickly a thin molten layer that is rapidly solidified (see Fig. 1). The heat transfer and solidification of the molten metal can then be treated in a one-dimensional manner (Fig. 2), because the splat thickness is much smaller than the dimensions in other directions. An electromagnetic levitation system was used to melt pure nickel or copper droplets without contact with any solid surface. The molten droplet of a diameter of about 4–6 mm was then dropped on an inclined cold substrate to form a thin splat. As the liquid splat cools down and solidifies, the temperature of the top surface was measured by a one-color pyrometer. The whole setup is enclosed in a stainless steel chamber filled with an argon and helium mixture.

The one-color IR pyrometer used (IRCON 1100) has a response time of about 1.5 ms and a temperature range from 1573 to 2173 K. The pyrometer was connected to a data-acquisition system controlled by a computer. A two-color pyrometer with a response time of about 25 ms was also used to measure the temperature of the molten copper droplet while levitating. The initial substrate temperature was measured by a K-type thermocouple attached to the top substrate surface close to the location where the molten metal droplet impacts.

After each experiment, a micrometer was used to determine the splat thickness, b, by measuring the average thickness in the area viewed by the pyrometer. This is necessary because the splat thickness can vary significantly from the edge to the center. The analog readings of the single-color pyrometer were then converted into temperatures using an emissivity value determined based

on the equilibrium melting points of the melting materials (nickel and copper), as described below.

Four metallic substrates were prepared for the present experiments: copper, aluminum, steel (AISI 1080), and stainless steel (AISI 440C). The substrates were machined to 76 mm × 38 mm × 12.5 mm (except for the stainless steel ones, which are only 10 mm in thickness). All of the substrates were first surfaced by a grinder (a finish referred to hereafter as "Ground" surfaces). Some of them were then further polished using abrasive papers of 240 and 600 grit. Some of the substrate surfaces were bead-blasted. Two sizes of beads were used: coarse beads with diameters ranging from 406 to 432 μm ("Blasted-C" surfaces) and fine beads of 89–150 μm diameter ("Blasted-F" surfaces). Two additional surfaces were also prepared for the copper substrates: a "Rough #1" surface as sawn, and a "Rough #2" surface which was first end-milled and then finished with a steel brush wheel. The arithmetic average roughness R_a of each substrate was measured by a stylus profilometer (DEKTAK IIA, Sloan Technology). The diamond stylus tip diameter is 12.5 μm. The scanning length is 5.0 mm. The surface roughness data are given in Tables 2–5.

To convert the pyrometer output into temperature readings, one needs to know the surface emissivity of the splats. Little information is available for the emissivity of liquid metals, however. In the case of copper, calibration experiments were performed to determine the surface emissivity of liquid copper and solidified copper surface using a small ingot in an alumina crucible [13,14]. The temperature of the copper ingot was measured by both a thermocouple and a pyrometer. The comparison between the two provides information on the surface emissivity of the liquid and solidified solid copper. The copper ingot experiments showed that the solidification plateau seen in the splat cooling curve can give a good estimate of the surface emissivity of both the liquid and solidified solid copper. Based on these findings, the surface emissivity of the liquid and solidified nickel was estimated based on the solidification plateau in the nickel splat cooling curve, as shown in Fig. 3. Fig. 3a shows the pyrometer output when a molten nickel droplet free-falls on a horizontal copper substrate. Since the impacting velocity is relatively small (a few meters per second), a rather thick splat of about 1 mm in thickness was formed. As one can see in Fig. 3a, the pyrometer output shows clearly a plateau indicating an isothermal solidification. It also shows clearly the end of solidification. Since pure nickel was used in the experiment, the plateau in Fig. 3a corresponds to the equilibrium melting temperature of the pure nickel, $T_M = 1726$ K. Based on this temperature, one could estimate a value of 0.268 for the surface emissivity of nickel for both liquid and solid surfaces. If we assume further that the surface emissivity does not change significantly with temperature, one can then use this emissivity to obtain temperature data during the entire cooling process as shown in Fig. 3b. For the cases when a thin splat was formed on an inclined substrate, the end of the solidification plateau was sometimes less obvious, as shown in Fig. 4a. In that case, some error is introduced in the temperature data for the solid cooling period. As the primary focus of the present work is on the interfacial heat transfer during the early stages of melt cooling and solidification, such an error can be tolerated. For all nickel splats considered, a rather consistent value, ranging from 0.25 to 0.27, was found for the

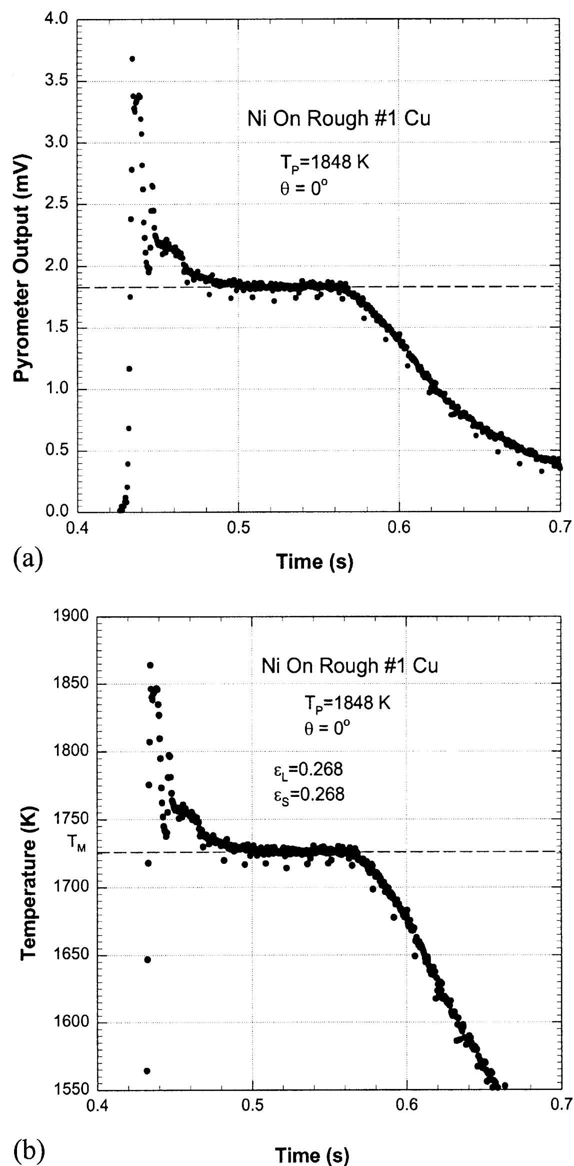

Fig. 3. (a) Pyrometer readings and (b) conversion to temperature. Note that the liquid and solid emissivities can be determined based on the known equilibrium melting temperature of the metal.

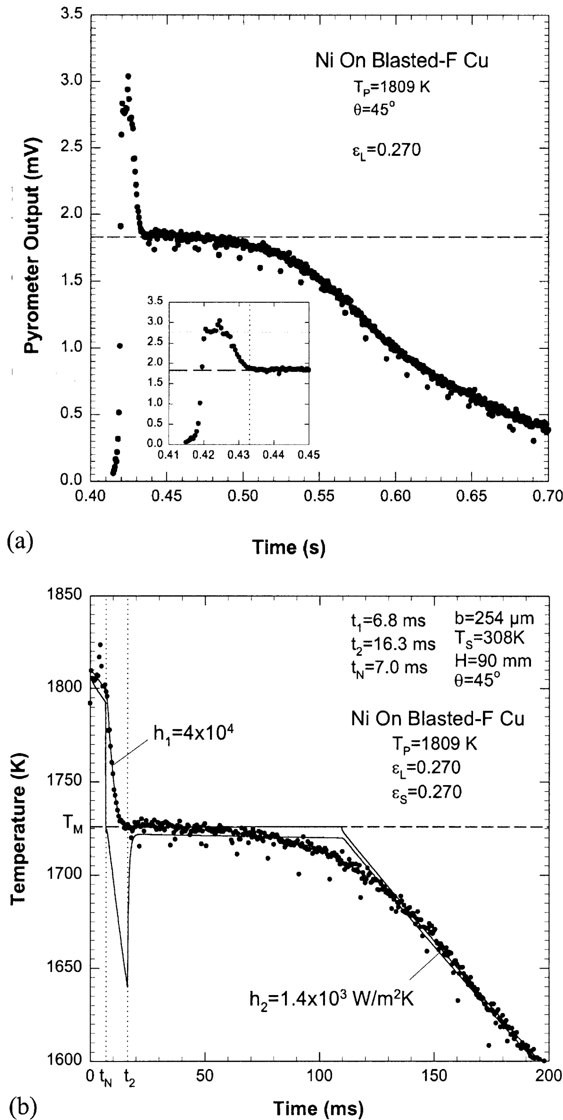

Fig. 4. (a) Pyrometer readings; (b) the converted temperature variation of the splat top surface (solid dots) as well as the corresponding model calculations (upper solid line—calculated temperature of the splat top surface, lower solid line—calculated temperature of the splat bottom surface). Note the good match between the calculations and measurements.

emissivity of liquid nickel surfaces. For solid surfaces, however, the values ranged from 0.15 to 0.27, depending on the splat surface condition. The emissivity of copper was also estimated and is reported on elsewhere [13].

3. One-dimensional solidification model and procedure for estimation of *h(t)*

A temperature matching method is used to estimate the interfacial heat transfer coefficient for each splat experiment [14]. The splat cooling and subsequent solidification shown in Fig. 1 can be analyzed with a one-dimensional model developed previously [15] and illustrated in Fig. 2. The model simulates a thin molten metal layer that is suddenly put in contact with a colder substrate. An interfacial heat transfer coefficient is introduced at the interface between the layer and the substrate. The model can be solved numerically for any given splat thickness (b), the initial temperatures of the molten metal (T_p) and the substrate (T_S), and the interfacial heat transfer coefficient (h), in order to obtain the variations of the temperature T_{ST} of the splat top surface. For fixed values of b, T_p, and T_S, different values of h will result in different splat surface temperatures. By matching the model-predicted temperature with the measured data, one can then estimate the interfacial heat transfer coefficient, h.

For a thin liquid layer on a semi-infinite substrate, the heat conduction equations in the solidifying metal and the substrate can be written as [15]:

$$\rho_j C_{pj} \frac{\partial T_j}{\partial t} = \frac{\partial}{\partial y}\left(K_j \frac{\partial T_j}{\partial y}\right) \tag{1}$$

where ρ is the density, C_p is the specific heat capacity, K is the thermal conductivity, y is the coordinate normal to the substrate surface, and the subscript j stands for the substrate, solid, or melt. Since the splat is rather thick (100–300 μm) in the cases considered here, no melt undercooling needs to be taken into account. Solidification is assumed to begin on the substrate surface at time t_N when the temperature of the molten metal at the surface reaches the equilibrium melting temperature, T_M, of the cast metal. A local equilibrium condition exists then at the moving solid/liquid interface, i.e. the interface temperature $T_i = T_M$. The solidification velocity, V_i, is then determined by the rate of latent heat removal at the interface:

$$\rho_L V_i L = K_L \frac{\partial T_L}{\partial y}\bigg|_i - K_S \frac{\partial T_S}{\partial y}\bigg|_i \tag{2}$$

where L is the latent heat of solidification. At the interface between the splat and the substrate, an interfacial heat transfer coefficient, h, is introduced:

$$h(t) = \frac{q(t)}{T_{sb}(t) - T_{ss}(t)} \tag{3}$$

where $q(t)$ is the heat flux through the contact interface from the splat to the substrate, $T_{sb}(t)$ is the average temperature at the splat bottom surface in contact with the substrate, and $T_{ss}(t)$ is the average temperature of the substrate surface. T_{sb} and T_{ss} do, of course, vary somewhat with location, and the interfacial heat transfer coefficient defined in Eq. (3) describes only an average heat transfer at the interface between the splat and the substrate. As the molten metal cools down and solidifies, the contact condition at the interface changes from a liquid-solid contact to a solid-solid contact, and it is

expected that the interfacial heat transfer coefficient varies strongly with time.

At the top surface of the splat ($y = b$) heat may be lost by both convection and radiation:

$$-K_j \frac{\partial T}{\partial y}\bigg|_{y=b} = h_\infty (T(b,t) - T_\infty) + \varepsilon\sigma\Big(T(b,t)^4 - T_\infty^4\Big) \quad (4)$$

where h_∞ is the convective heat transfer coefficient between the splat surface and the surrounding gas, ε is the surface emissivity of the splat, and σ is the Stefan–Boltzmann constant. The substrate is treated as a semi-infinite body with the temperature far from the surface remaining constant: $T(-\infty, t) = T_S$. At the beginning of the process, $t = 0$, the splat is assumed to be at a uniform temperature T_p, and the substrate is at a uniform temperature T_S.

This mathematical problem can be solved using the control volume method, with a special treatment needed to deal with the moving interface. Details can be found elsewhere [13–15].

For any given splat thickness b, and initial temperatures T_p and T_0 of the splat and the substrate, the model can calculate the variation of the splat temperature, if the interfacial heat transfer coefficient $h(t)$ is known. Conversely, if one knows the splat temperature history, the interfacial heat transfer coefficient can then be estimated, but the inverse heat transfer problem is ill-posed, mathematically speaking [5–7]. The accuracy of the estimated value of $h(t)$ depends on the locations where the temperature information is acquired, and the closer this location is to the interface, the more accurate is the estimated $h(t)$. In these experiments, it is the temperature at the splat top surface that is measured. Such temperature information does not therefore guarantee an accurate estimate of a continuously varying $h(t)$ as a function of time, and as a result, only an average value of $h(t)$ over short time periods was estimated. Indeed, we divided the splat cooling and solidification process into three or four time periods, and an average value of $h(t)$ could be estimated for each time period by matching the model-calculated splat surface temperature to the experimental data.

In our previous work with copper splats [13], the entire splat cooling process was divided into four time periods with corresponding values of h: (1) initial melt spreading (h_0), (2) liquid splat cooling (h_1), (3) solidification (h_2), and (4) solid cooling (h_3). It was found that such a division provides a well-defined average value of $h(t)$ over each period. For the nickel splats considered primarily in the present work, it was found that a good match can be achieved in most cases by using only two time periods after the initial spreading: the time period covering the liquid splat cooling and the early stages of solidification (h_1) and the time period afterwards (h_2).

Table 1
Physical properties of materials used in the calculations

	Ni[a]	Cu[a]	Al[a]	Steel[b]	SS[b]
T_M (K)	1726				
L (J/kg)	2.9×10^5				
C_{pL} (J/kg K)	620				
C_{pS} (J/kg K)	595	389	984	548	460
λ_L (W/m K)	43				
λ_S (W/m K)	80	394	238	46.8	24.2
ρ_L (kg/m^3)	7900				
ρ_S (kg/m^3)	8450	8900	2700	7800	7800

[a] [19,20].
[b] [21].

Since the splat thickness keeps decreasing during spreading but the temperature remains almost the same, the estimated h_0 during this early spreading period is not very meaningful and will therefore not be included in discussion.

Fig. 4 shows typical temperature measurements and matching predictions for a nickel splat with an original 83 K melt superheat dropped on a fine-bead-blasted copper substrate (Blasted-F) inclined at 45°. The free fall distance of the molten droplet is $H = 90$ mm. A constant emissivity of 0.270, estimated from the isothermal plateau, is used to convert the original pyrometer readings into the temperature data. The materials properties used in the calculations are listed in Table 1.

As shown in Fig. 4b, the splat cooling process was divided into three regions, each being represented by a constant value of h: h_0 for the period from 0 to $t_1 = 6.8$ ms, h_1 from t_1 to $t_2 = 16.3$ ms, and h_2 after t_2. As one can see, a good match between the model predictions (solid lines) and the measurements (solid dots) is achieved if we use $h_1 = 4 \times 10^4$ W/m^2 K and $h_2 = 1.4 \times 10^3$ W/m^2 K. (In the calculations, $h_0 = 1.5 \times 10^3$ W/m^2 K was also used, but since h_0 is not physically meaningful due to melt spreading, it will not be included in the discussions hereafter.) The model calculations suggest that solidification starts at about $t_N = 7.0$ ms which is very close to the time $t_1 = 6.8$ ms when spreading ends, suggesting that h_1 corresponds mainly to a solid/solid contact at the splat/substrate interface, and little information can be generated for the initial liquid/solid contact in this particular case.

More examples of the matched cooling curves are given in Figs. 5–7. Using the same matching method, the interfacial heat transfer coefficient has been evaluated for all splat cooling experiments and is given in Tables 2–5. With these results, one can examine the dynamic features of the interfacial heat transfer during the splat cooling, and the effect of the processing conditions, such as melt superheat, substrate material, and surface roughness, on the average value of h.

The uncertainty on the estimated h_1, and h_2 results primarily from the uncertainties in splat thickness b,

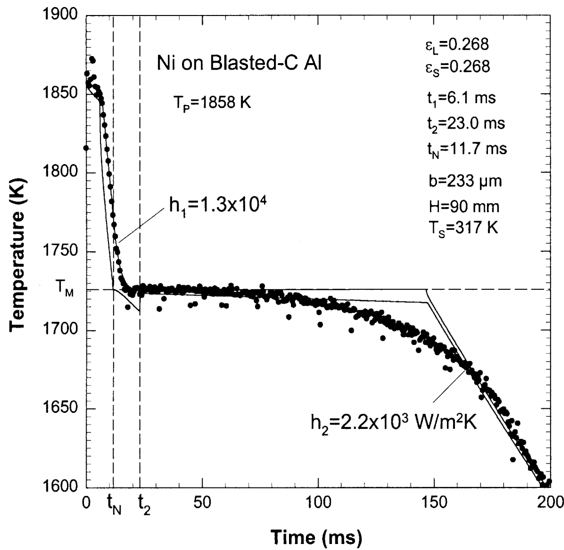

Fig. 5. Matching of numerical predictions with experimental data for nickel on an inclined Blasted-C Al substrate. Solid dots—experimental data, upper solid line—calculated temperature of the splat top surface, lower solid line—calculated temperature of the splat bottom surface. (T_p = 1858 K, b = 233 µm, H = 90 mm, $\theta = 45°$, T_S = 317 K, ε_L = 0.268, ε_S = 0.268).

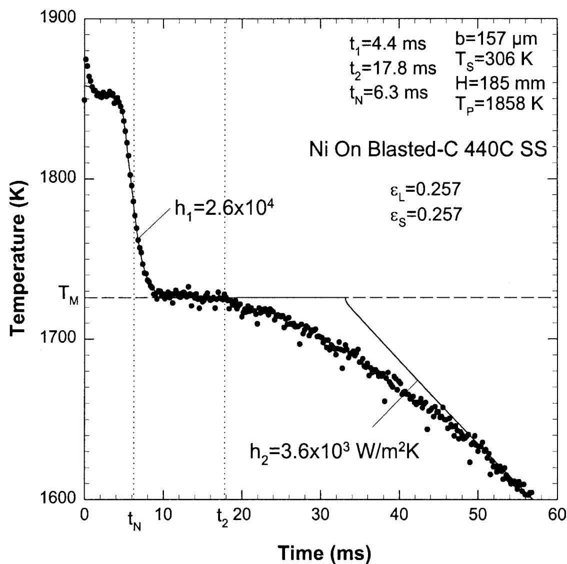

Fig. 6. Matching of the numerical predictions with experimental data for nickel on an inclined Blasted-C 440C stainless steel substrate. Solid dots—experimental data, solid line—calculated temperature of the splat top surface. (T_p = 1858 K, b = 157 µm, H = 185 mm, $\theta = 45°$, T_S = 306 K, ε_L = 0.257, ε_S = 0.257).

initial melt temperature T_p, substrate temperature T_S, and the temperature matching process itself, with the other parameters contributing to a smaller extent. The

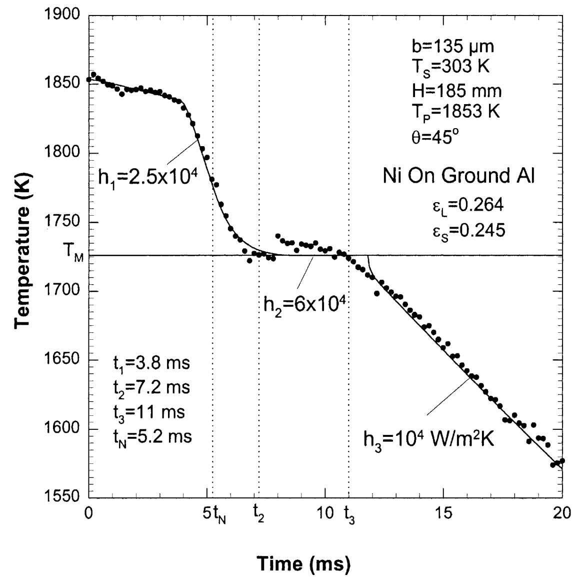

Fig. 7. Matching of numerical predictions with experimental data for nickel on a ground Al substrate. Solid dots—experimental data, solid line—calculated temperature of the splat top surface. (T_p = 1853 K, b = 135 µm, H = 185 mm, $\theta = 45°$, T_S = 303 K, ε_L = 0.264, ε_S = 0.245).

Table 2
Estimated h for a nickel splat cooling on copper and aluminum substrates (H = 90 mm, $\theta = 45°$)

Substrate	R_a (µm)	T_p (K)	h_1 (10^4 W/m^2 K)	h_2 (10^4 W/m^2 K)	b (µm)
Cu Grit #600	0.07	1763	5.5	0.12	242
		1820	15	0.7	419
		1920	30	0.72	410
Cu Ground	0.29	1863	10	0.12	365
Cu Blasted-F	1.80	1809	4.0	0.14	254
		1873	9.0	0.8	299
Cu Blasted-C	2.88	1858	4.5	1.7	229
		1909	8.5	1.7	259
Al Grit #240	0.29	1766	1.2		266
		1874	2.5	0.11	231
Al Ground	0.39	1813	0.9		199
		1861	1.5	0.13	186
Al Blasted-F	1.04	1823	1.5	0.04	213
		1868	1.9	0.12	248
Al Blasted-C	1.12	1761	3.0		272
		1818	2.5	0.17	252
		1858	1.3	0.22	233
		1905	3.2	0.083	259

uncertainty on the initial melt temperature T_p results in turn mainly from the uncertainty in the estimated surface emissivity ε. The relative uncertainties on the splat thickness, surface emissivity, and substrate temperature are estimated to be about 0.20, 0.10, and 0.05,

Table 3
Estimated h for a nickel splat cooling on copper, steel, and stainless steel substrates ($H = 185$ mm, $\theta = 45°$)

Substrate	R_a (μm)	T_p (K)	h_1 (10^4 W/m^2 K)	h_2 (10^4 W/m^2 K)	b (μm)
Cu Grit #600	0.07	1842	16		243
		1859	26	0.65	283
Cu Ground	0.29	1858	6.0	0.55	182
		1848	8.0	0.7	204
Cu Blasted-F	1.80	1848	10.0	0.2	206
		1865	4.0	0.15	207
Cu Blasted-C	2.88	1853	10.0	0.1	215
		1845	6.0	0.4	173
		1853	4.0	0.4	201
Cu Rough #2	5.19	1863	10	0.46	300
Cu Rough #1	7.68	1858	4.0	0.6	200
Steel Ground	0.17	1846	12.0	0.7	211
		1848	9.0	0.6	189
Steel Grit #240	0.29	1858	4.0	0.4	256
		1858	2.0		177
Steel Blasted-F	0.60	1845	4.0	0.35	176
		1843	4.5	0.62	155
Steel Blasted-C	1.49	1845	3.5	0.75	163
		1852	4.0	0.7	154
SS Ground	0.19	1853	8.0	0.7	239
		1853	2.1	0.75	124
SS Blasted-F	0.29	1853	1.2	–	135
		1858	2.2	0.45	156
SS Blasted-C	0.78	1858	2.6	0.36	157

respectively. Using a standard uncertainty analysis procedure, and considering also the possible errors introduced by the matching process itself, the maximum uncertainty in h_1 is estimated to be about 100%, and that in h_2 is about 44% [14]. Considering the complexity of this interfacial heat transfer problem involving solidification, those numbers should be acceptable.

4. Experimental results and discussions

Our experiments involved two cast materials: nickel and copper; and four substrate materials: copper, aluminum, steel, and stainless steel. Two droplet free-fall heights H were used: 90 and 185 mm. In all cases, the substrate was inclined at 45° to help generate thin splats. The processing conditions focused on here are the melt superheat, the substrate material, the substrate surface roughness, and the cast material.

4.1. Variation of h during nickel splat cooling

Before we examine the effect of the processing conditions on the interfacial heat transfer, it is interesting to examine the dynamic characteristics of $h(t)$ during the process. In a previous article on copper splat cooling [13], a three-steps variation in interfacial heat transfer coefficient had been assumed for the temperature matching method, each representing an average value over time: h_1 for the initial melt cooling period, h_2 for the isothermal solidification period, and h_3 for final solid phase cooling. (The initial melt spreading time period was not considered.) In that case, we found four types of variation in h: (1) $h_1 = h_2 > h_3$; (2) $h_1 > h_2 > h_3$; (3)

Table 4
Estimated h for a nickel splat cooling on aluminum substrates ($H = 185$ mm, $\theta = 45°$)

Substrate	R_a (μm)	T_p (K)	h_1 (10^4 W/m^2 K)	h_2 (10^4 W/m^2 K)	h_3 (10^4 W/m^2 K)	b (μm)
Al Grit #600	0.18	1853	3.5	4.0	0.6	212
		1855	3.0	3.9	0.4	200
Al Ground	0.39	1843	2.0	3.0	0.7	114
		1853	2.5	6.0	1.0	135
Al Blasted-C	1.12	1846	2.0	4.6	0.6	132

Table 5
Estimated h for a Cu splat on various Cu substrates ($H = 185$ mm, $\theta = 45°$)

Substrate (Cu)	R_a (μm)	T_p (K)	h_1 (10^4 W/m^2 K)	h_2 (10^4 W/m^2 K)	h_3 (10^4 W/m^2 K)	b (μm)
Grit #600	0.07	1523	9.0	0.08	0.08	266
Ground	0.29	1523	8.0	0.1	0.1	241
Blasted-F	1.80	1518	6.0	0.12	0.12	251
Blasted-C	2.88	1522	6.0	0.1	0.1	217
		1528	6.0	0.09	0.09	234
Rough #2	5.19	1518	5.0	5.0	0.3	222
Rough #1	7.68	1519	4.8	0.3	0.3	236

$h_1 \gg h_2 = h_3$; and (4) $h_1 < h_2$ (with $h_1 > h_3$ and $h_2 > h_3$); depending on the melt superheat, substrate material, and surface condition. Examining the estimated h values in Tables 2–5, we see the third kind of pattern for most of nickel splats, i.e. a much larger h_1 followed by small equal h_2 and h_3. This indicates that the contact condition at the interface remains relatively unchanged during liquid cooling and the earlier stages of splat solidification. The contact condition at the interface, however, sees a dramatic change—in the middle of—or near the end of solidification, probably because of the thermal stresses that lead to separation of the splat from the substrate and therefore to a much lower value of h.

A type 4 variation of h is, however, also observed for nickel splat cooling on aluminum substrates as shown in Fig. 7 and also Table 4. In this case, a three-steps variation of h must be used in order to achieve a close match between the calculations and the measurements. In particular, a larger h_2 during the solidification period must be used in order to have appropriate match between the calculated total solidification time and the measured one. As pointed out previously [13], this kind of variation of the interfacial heat transfer coefficient is not expected from simple thermal contraction mechanisms, and it might be related to substrate heating, gas expansion or contraction in interstices, etc., at the interface.

Further insight in the contact physics at the interface and in the dynamic behavior of the interfacial heat transfer may also be achieved by examining the time variations of the calculated temperature in the splat. Fig. 4b shows the temperatures variation at the top and bottom surfaces of the nickel splat quenched on a Cu substrate. It is seen that the calculated nucleation time t_N is very close to the estimated time at which melt spreading ends. This suggests that the high value of h_1, 4×10^4 W/m^2 K, reflects primarily a solid/solid contact condition. One might think that an even better interfacial contact condition exists during the earlier liquid/solid contact, but could not be evaluated accurately by the present experimental technique. (In the case of Fig. 4b, the initial time period during which a liquid/solid contact exists overlaps with the interval during which the melt is spreading and the splat is forming. As mentioned above, during this period of time our one-dimensional model is not applicable because of the varying splat thickness and the existence of melt flow.) Some other experimental results suggest, however, that this estimated h_1 value does represent, at least in an average sense, the initial liquid/solid contact conditions as well. This may be seen by referring to Fig. 5, which shows the measured temperature history of the splat top surface and the temperature calculations for nickel on a coarse bead-blasted aluminum surface. In this case, the melt spreading process ended before the calculated nucleation time t_N is reached ($t_1 = 6.1 < t_N = 11.7 < t_2 = 23.0$ ms). In other words, the matched h_1 in this case should correspond to both liquid/solid contact before solidification and solid/solid contact after solidification. It is interesting to note that the transition from a liquid/solid to a solid/solid contact does not appear to be reflected by any discontinuity in the measured splat surface cooling curve. A good match was also obtained between the calculations and the measured temperatures by using a single value of h through the transition, which suggests a stable contact condition during this period of time. This may further suggest that the crystalline nucleation on the substrate surface does not immediately change dramatically the thermal contact condition at the interface, and that the variation of the thermal contact condition there results from other mechanisms, e.g. solid contraction during cooling.

An examination of Fig. 4b also suggests that a very large temperature difference exists in the splat during the earlier stages of the process, e.g. about 85 K across the splat when the splat top surface temperature reaches melting temperature at about $t = 16$ ms. This large temperature difference across the splat cannot be sustained when the interfacial heat transfer changes from the higher h_1 to a much lower h_2 at the transition time $t_2 = 16.3$ ms, however. As seen in the figure, a sharp temperature increase of the splat bottom surface is calculated, and in a very short time (2–3 ms) the splat bottom surface temperature reverts to close to melting temperature. This sharp variation of the calculated splat bottom surface temperature is, of course, an artificial result of the assumption of a sudden change from a higher h_1 to a lower h_2, and in reality, the variation of h is likely much more gradual and so is the splat bottom surface temperature variation.

4.2. Effect of the melt superheat on h for nickel splats

We investigated how the melt superheat affects the interfacial heat transfer between the solidifying splat and the substrate. For instance, melt with a higher superheat typically has a smaller viscosity and surface tension, and therefore may have a better contact with a rough surface. As the melt superheat increases, uniform splats become less likely to form, however. This is particularly true on substrates made of stainless steel and carbon steel. As the temperature becomes higher, oxidation becomes more significant, which makes it more difficult for the nickel melt to wet the substrate surface. As a result, only limited data were obtained for those substrates.

Fig. 8a and b show h_1 and h_2, respectively, as a function of melt superheat for substrates made of copper and aluminum with various surface roughness

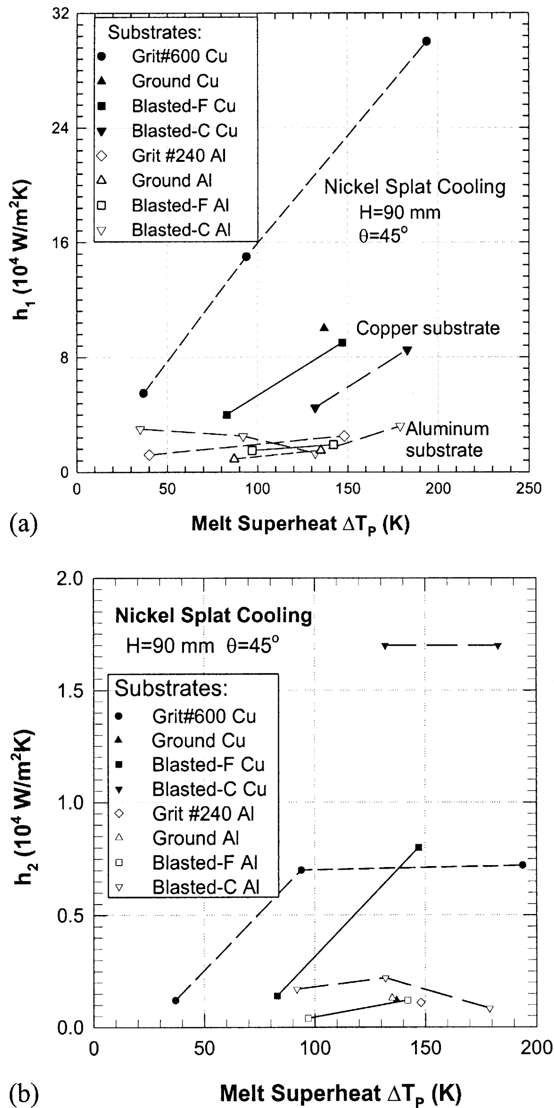

Fig. 8. Estimated interfacial heat transfer coefficients for h_1 (a) and h_2 (b) as a function of the melt superheat ΔT_p for a nickel splat on four copper and four aluminum surfaces. ($H = 90$ mm, $\theta = 45°$).

conditions. All data are listed in Table 2 and were obtained with substrates being inclined at 45° under a free-fall distance of $H = 90$ mm.

Some observations can be derived from Fig. 8a. First, the substrate material has a profound effect on the value of h_1. A much higher value of h_1 is seen for nickel on a copper substrate than on an aluminum substrate. For the conditions studied here, h_1 ranges from 4×10^4 to 30×10^4 W/m^2 K for nickel on copper substrates, but only from 1×10^4 to 3×10^4 W/m^2 K on aluminum substrates. For example, for similar melt superheat (about 150 K) and a ground surface roughness, h_1 is about 10×10^4 W/m^2 K on a copper substrate but only about 2×10^4 W/m^2 K for an aluminum substrate, a five times ratio. This effect of substrate material on h_1 results likely from the difference in chemical compatibility of the nickel metal with copper and aluminum.

Fig. 8a also shows a strong effect of the melt superheat on h_1 for copper substrates, with a higher melt superheat giving a higher value of h_1. The largest increase in h_1 was observed for the smoothest copper surface (Grit #600-Cu) used: a six-fold increase in h_1 when the melt superheat increases from 40 to 190 K. The increase of h_1 with the melt superheat is, however, affected by the surface roughness. For rough substrates, the superheat has a weaker effect on h_1. It is interesting to note that this observation may be contrary to intuition since a stronger effect of the melt superheat could be expected on a rougher surface than on a smooth surface, given that a highly superheated melt could presumably conform more easily to the rough surface, leading therefore to a better contact. Under these experimental conditions, however, the interface heat transfer may also be influenced greatly by the gas pockets entrapped underneath the splat bottom surface. A rough surface may trap more gas pockets than a smooth surface, resulting in a smaller affective contact surface and therefore in a smaller value of h_1. This phenomenon is more visible on a copper substrate than on an aluminum substrate. In the case of an aluminum substrate, increasing the melt superheat also led in most cases to an increase in h_1, but much less so than for copper substrates. Except for the roughest surface, Blasted-C Al, all three surfaces show a similar rate of increase in h_1 with increasing melt superheat. In the case of the Blasted-C Al substrate, increasing the superheat leads to a reduction in h_1 for superheats smaller than about 150 K.

The effect of the melt superheat on the interface heat transfer h_2 during the later stages of nickel splat cooling is shown in Fig. 8b for both copper and aluminum substrate surfaces. Except for the coarse bead-blasted copper surface, the values of h_2 are all under 10^4 W/m^2 K. The effect of the melt superheat on h_2 shows no clear trend in these tests. For some substrate surfaces, such as the Blasted-F copper and aluminum surfaces, an increase in the melt superheat increases h_2. A similar effect is seen for polished copper surface (Grit #600 Cu) at low melt superheat, but no such effect can be seen when the superheat is large. Rather large h_2 values were obtained for nickel quenched on a blasted (Blasted-Coarse) copper substrate but no melt superheat effect can be seen in that case. In addition, it appears that no clear trend can be seen for the effect of surface roughness on h_2. On the other hand, the substrate material seems to have a certain effect on h_2, as larger values of h_2 are generally seen for the copper surfaces than for the aluminum surfaces.

4.3. The effect of the surface roughness on h

The effect of the substrate surface roughness on h_1 has also been investigated more quantitatively. The melt superheat was kept at about the same level for given material pairs, and a high melt superheat was generally used to obtain more temperature data points in the liquid cooling region. Meaningful data were obtained when nickel was quenched on four substrate materials. For copper splats, valid data were obtained only for copper substrates, as most copper splats formed on substrates other than copper usually contained many small holes.

The estimated interfacial heat transfer coefficients (h_1 and h_2) for nickel splats on copper, steel, and stainless steel are listed in Table 3 together with the corresponding substrate surface roughness and the splat thickness. The estimated interfacial heat transfer coefficients for nickel splats on the aluminum substrates are given in Table 4, and in this case a three-steps variation of h must be used in order to achieve close match between the calculations and the experimental measurements. Table 5 lists the data for copper droplets on a copper substrate, and as in the case of the aluminum substrates, a three-steps variation was used in the temperature matching process. For most cases, however, h_2 and h_3 are the same.

In most cases, two or three runs were made for the same substrate roughness in order to check the repeatability of the process, and for some metals a significant scattering in the estimated h_1 values was noted. Even so, a clear trend can be seen in the data for h_1. No such trend can be seen, however, for h_2, and no discussion of h_2 will be attempted hereafter. All these experiments have been performed with $H = 185$ mm and $\theta = 45°$.

4.3.1. Copper splats quenched on copper substrates

Table 5 lists all the estimated interfacial heat transfer coefficients (h_1, h_2, and h_3) for the conditions studied. Six different surface conditions of copper substrate were used with the surface arithmetic average roughness R_a ranging from 0.07 μm (Grit #600) to 7.68 μm (Rough #1).

Two runs on Blasted-C surfaces have been performed, and, as seen in the table, very similar interfacial heat transfer coefficients have been calculated even though the melt superheat and the splat thickness are a little different. Similar comparisons have also been performed in other cases, and all the results confirmed that the calculated interface heat transfer coefficients have a rather good repeatability when copper is quenched on various substrates.

In all cases listed in Table 5 except for the Rough #2 surface, we see a h_1 much larger than h_2 and h_3, both of which are the same (a Type 3 pattern). For the Rough

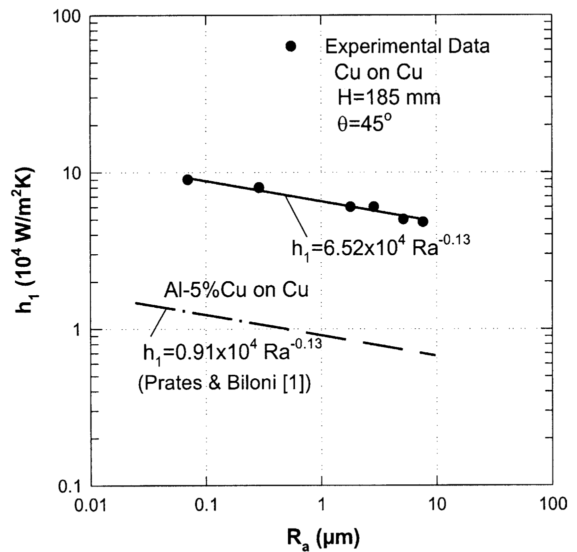

Fig. 9. Estimated interfacial heat transfer coefficient h_1 (10^4 W/m^2 K) as a function of the arithmetic average roughness R_a of the substrate surface for copper splats quenched on copper substrates ($T_p = 1520$ K, $H = 185$ mm, $\theta = 45°$).

#2 surface, the variation of h is a Type 1 (same h_1 and h_2).

The effect of the surface roughness on the interfacial heat transfer coefficient h_1 can be more easily visualized in Fig. 9 which plots h_1 as a function of R_a. (Note the logarithmic scales used in these figures). As seen in Fig. 9, h_1 is affected by the surface conditions: the smoother the surface, the better the thermal contact, and the higher the value of h_1. As the surface roughness decreases from 7.68 to 0.07 μm, h_1 increases from 4.8×10^4 to 9×10^4 W/m^2 K, almost a factor of 2. The data can be fitted quite well by a power–law relationship between h_1 (W/m^2 K) and R_a (μm) as follows:

$$h_1 = C_1 R_a^n \tag{5}$$

with the constant $C_1 = 6.52 \times 10^4$ and the exponent $n = -0.13$.

Interestingly, the same power–law relationship was also observed by Prates and Biloni [1] who cast an Al–5%Cu alloy on a bare copper mold with varied surface roughness. They polished the copper surfaces with emery paper of various grit number, and the resulting surfaces had roughness ranging from 0.02 to 6.0 μm root mean square. The corresponding arithmetic average roughness R_a ranges approximately from 0.016 to 4.8 μm if it is assumed that the surface profile can be approximated as a symmetrical Gaussian distribution [17]. Prates and Biloni estimated h using a linear fluidity test with a low channel height and derived a relationship between h and R_a with the same exponent −0.13 as our

Eq. (5). In their case, however, the constant C_1 is only 0.91×10^4. This relationship is shown by a dashed line in Fig. 9. Realistically, the same exponent of −0.13 observed in both cases may be just a coincidence though, considering the uncertainties in the measured surface roughness, the different system configurations, and the different thermal contact conditions. These relationships do, however, demonstrate the dependency of the interface heat transfer coefficient on the surface roughness.

4.3.2. Nickel splats on different substrates

Fig. 10 shows the estimated h_1 as a function of the substrate surface roughness R_a for a nickel splat cooling on three substrate materials: copper, aluminum, and steel (AISI 1080). (There is large uncertainty in the estimated h_1 for stainless steel substrate, so the data is not included here.) We see a large scattering in the estimated h_1, especially when nickel is quenched on a copper substrate with large R_a. (This is different from the case of copper on copper for which repeatability is excellent.) For example, when nickel was quenched on a Blasted-C copper substrate, the estimated h_1 varied from 4×10^4 to 10×10^4 W/m^2 K, about a factor of 2. It should be pointed out that this range is much larger than that predicted by our uncertainty analysis, which suggests that some factors other than those directly controlled in our experiments may have a strong effect on thermal contact as well. These factors could result, for example, due to surface oxidation from residual oxygen in the vacuum chamber.

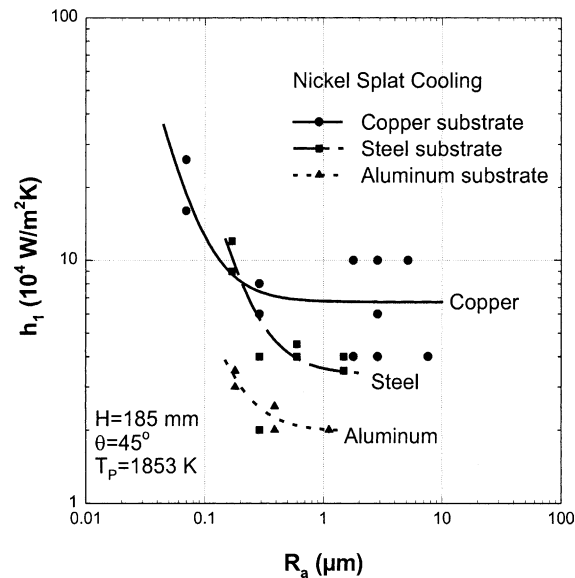

Fig. 10. Estimated interfacial heat transfer coefficient h_1 (10^4 W/m^2 K) as a function of the arithmetic average roughness R_a of the substrate surface for nickel on three substrates: copper, steel, and aluminum. ($T_p = 1853$ K, $H = 185$ mm, $\theta = 45°$).

Nevertheless, a clear trend for the dependency of h_1 on the substrate surface roughness R_a may still be noted in Fig. 10. For all three substrate materials, similar variations of h_1 with the surface roughness R_a can be seen. In all cases, when R_a is large, h_1 has a rather small dependency on the surface roughness R_a, but when R_a is small, decreasing R_a will dramatically increase h_1. It is noted that similar variations of the interfacial heat transfer with substrate roughness has also been observed in twin-roll casting of steel [16]. In the present case, the maximal value of R_a at which its effect on h_1 can still be seen appears to be about $R_a = 0.5$ μm for nickel splat cooling, and about the same for the other substrate materials as well. This suggests that the transition to h_1 being independent of R_a is controlled primarily by the surface tension of the liquid splat metal. The same type of correlation can be obtained by curve-fitting the experimental data for the three substrate materials:

$$h_1 = C_1 R_a^n + C_2 \tag{6}$$

with different values of constants C_1 and C_2 but with the same exponent $n = -2$. Table 6 shows the fitted constants for three substrate materials, with h_1 given in W/m^2 K and R_a in μm. The constant C_2 represents the asymptotic value of h_1 at large R_a. Evidently, there is a strong dependence of this asymptotic value on the substrate materials. As we can see, the copper surface gives the highest value of C_2, the steel surface is second, and the aluminum surface has the lowest C_2 of the three. As is also seen in Fig. 10, even though the exponent of R_a in the Eq. (6) is the same, the absolute variation of h_1 with R_a is quite different for the different substrate materials, as quantified by rather different values of C_1.

Caution must be exercised as far as the constants in Table 6 are concerned, however. Because a rough surface typically exhibits a multiscale structure but the R_a is a scale-dependent parameter, the measured R_a value may strongly depend on the measuring instrument and on the sample interval used [16]. Nevertheless, the relative variations of h_1 with the surface roughness, and the trends seen in Fig. 6 should likely remain valid regard-

Table 6
Constants in curve-fitted Eqs. (5) and (6) for various metals and substrates

Metal	Substrate	C_1	C_2	n
Nickel	Copper	0.07×10^4	6.70×10^4	−2
	Steel	0.198×10^4	3.38×10^4	−2
	Aluminum	0.042×10^4	1.97×10^4	−2
Copper	Copper	6.52×10^4	0	−0.13
Al–5%Cu[1]	Copper	0.91×10^4	0	−0.13

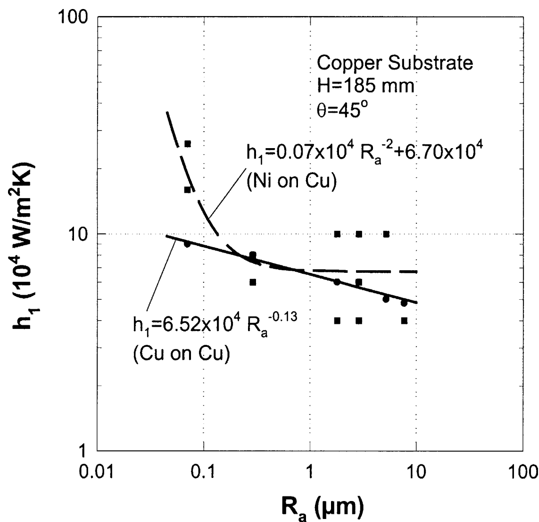

Fig. 11. Comparison of the variation of h_1 (10^4 W/m^2 K) versus R_a for nickel splats and copper splats quenched on copper substrate ($H = 185$ mm, $\theta = 45°$).

less of the absolute accuracy of the surface roughness measurements.

4.3.3. The effects of the type of cast metal on h

A comparison of h_1 obtained for both nickel and copper droplets quenched on the same copper substrates is shown in Fig. 11. As can be seen, when $R_a > 0.5$ μm both metals show almost the same h_1. The difference in h_1 between the two metals is greater when the surface roughness is smaller than about 0.5 μm, although there is only one set of data for copper in this region, which limits the generality of this observation. Interestingly—and perhaps contrary to some expectations—, a better thermal contact with the copper substrate was achieved for nickel splats than for copper splats when the copper substrate surface is very smooth.

The notion that similar thermal contact was achieved for both nickel and copper splats on copper substrates with large R_a has been further supported by examinations of the contact patterns seen on the bottom surfaces of the splats. It was observed that the bottom surfaces of both nickel and copper splats—when generated on the same rough substrates (such as Rough #1, Rough #2, and Blasted-C surfaces)—are very rough themselves and very similar. In these cases, it appears that the splat bottom surfaces are near mirror images of the substrate surfaces. No obvious marks of gas entrapment in these surfaces were seen for both nickel and copper splats on Rough #1 and #2 surfaces as well as for the nickel splat on the Blasted-C surface. Some small line-type gas pockets were, however, occasionally observed on the bottom surfaces of the copper splats generated on the Blasted-C surface.

The bottom surface of nickel splats generated on smoother substrates, such as the Blasted-F, Ground, and Grit #600 ones, have very different surface features from that of copper splats on the same surfaces. Continuous and web-like gas pockets (centered at the impacting point of the splat) can be clearly seen on the bottom surfaces of all the copper splats generated on those smoother surfaces, but no obvious marks of gas pockets can be seen on most of the nickel splats generated on the same surfaces (except that some isolated air pockets can be seen with the naked eye on the nickel splats obtained on the Blasted-F surface). This difference in surface features between the nickel and copper splats generated on the same substrate surface is likely to reflect a difference in the nature of the contact process, which in turn would likely be the cause of the different interfacial heat transfer coefficient seen in the range of lower R_a.

The existence of the macroscopic gas pockets on the copper splat surface may be understood given its lower surface tension compared to nickel. In addition, the oxygen residues in the chamber environment may also greatly decrease the surface tension of the copper [18]. When the molten copper impacts on the substrate and then spreads, some gas underneath the melt could be trapped. If the substrate surface is rough, like for the Blasted-C, Rough #1 and #2 surfaces, these gas pockets could likely be uniformly redistributed in the recesses of the surfaces, that the melt cannot penetrate because of its surface tension. If the surface is smoother, on the other hand, there are not enough recesses for the gas to infiltrate, and it will be forced to move with the melt and form web-like gas pockets under the surface. On the other hand, in the case of a nickel splat on a smooth surface, it may not be as easy for its gas to be trapped because of the larger surface tension of the nickel melt, and, as the melt moves over the substrate, most of the gas may be expelled from underneath the splat. This would result in fewer macroscopic gas pockets seen on the splat surface. Of course, since even our "smooth" surfaces are still microscopically rough, some microscopic gas bubbles can still be seen with a microscope, but as the substrate surface becomes smoother, the size of these microscopic gas bubbles is noted to decrease.

5. Conclusions

A splat cooling experimental system was built to determine the interfacial heat transfer coefficient (h) for molten metal droplets quenched on a cold metallic substrate. The effects on h of some processing conditions such as the melt superheat, the substrate materials, and the substrate surface finish were systematically investigated, and the following conclusions can be drawn from our study:

(1) A larger h_1 (10^4–3×10^5 W/m^2 K) between the splat and substrate is estimated for the earlier stages of melt cooling and solidification, followed by a lower h_2 ($<10^4$ W/m^2 K) for the subsequent stages of the process, including the later stages of solidification and of solid phase cooling. This decrease in h may be a consequence of the thermal contraction of the splat.
(2) The interfacial heat transfer coefficient h_1 is found to be affected strongly by all the processing conditions studied (the melt superheat, the cast metals, the substrate materials, and the substrate surface conditions). No obvious relationship can be observed, however, between these process conditions and the interfacial heat transfer coefficient h_2 under the experimental conditions used.
(3) In most cases, increasing the melt superheat increases h_1, i.e. improves the thermal contact between the splat and the substrate. The effect of the melt superheat on h_1 appears to depend on the substrate material and the surface finish.
(4) A power–law relationship was obtained between h_1 and R_a for both copper and nickel splats. In the case of the nickel splats, the same exponent ($n = -2$) is found for all three substrate materials (copper, steel, and aluminum).
(5) For the nickel splat cooling, the roughness appears to have a weak effect on h_1 when the surface is rough, but a large one when the surface is smooth. This transition appears to take place at a critical surface roughness about 0.5 μm (arithmetic average), which seems mainly determined by the cast metal, and less so by the substrate material.
(6) The interfacial heat transfer coefficient h_1 is also strongly affected by the substrate material in the case of nickel splats. The asymptotic h_1 at large R_a decreases from about 6.7×10^4 to 2×10^4 W/m^2 K when the copper substrate is replaced by an aluminum substrate.

Acknowledgements

We would like to acknowledge gratefully the support of the US National Science Foundation (Grant no. DDM-8957733 to EFM), and Professor C. Levi (UCSB) for kindly making some of his equipment available to us. GX Wang also thanks the support of the College of Engineering, the University of Akron.

References

[1] M. Prates, H. Biloni, Variables affecting the nature of the chill zone, Metall. Trans. 3 (1972) 1501–1510.
[2] K. Ho, R.D. Pehlke, Metal-mold interfacial heat transfer, Metall. Trans. B 16B (1985) 585–594.
[3] Y. Nishida, W. Droste, S. Engler, The air-gap formation process at the casting-mold interface and the heat transfer mechanism through the gap, Metall. Trans. B. 17B (1986) 833–844.
[4] H. Mizukami, T. Suzuki, T. Umeda, W. Kurz, Initial stage of rapid solidification of 18-8 stainless steel, Mater. Sci. Engng. A 173 (1993) 363–366.
[5] G.-X. Wang, E.F. Matthys, Interfacial thermal contact during rapid solidification on a substrate, in: G.F. Hewitt (Ed.), Heat Transfer 1994, Proceedings of the Tenth International Heat Transfer Conference, vol. 4, IChem^E, Brighton, UK, 1994, pp. 169–174.
[6] T. Loulou, E.A. Artyukhin, J.P. Bardon, Estimation of thermal contract resistance during the first stages of metal solidification process: II—experimental setup and results, Int. J. Heat Mass Transfer 42 (1999) 2129–2142.
[7] W. Wang, H.-H. Qiu, Determination of thermal contact resistance during the rapid contact solidification process, in: Proceedings of ASME NHTC01, Anaheim, CA, 10–12 June, 2001, NHTC2001-20168 (CD).
[8] W. Liu, G.-X. Wang, E.F. Matthys, Thermal analysis and measurements for a molten metal drop impacting on a substrate: cooling, solidification, and heat transfer coefficient, Int. J. Heat Mass Transfer 38 (1995) 1387–1395.
[9] C.A. Muojekwu, I.V. Samarasekera, J.K. Brimacombe, Heat transfer and microstructure during the early stages of metal solidification, Metall. Mater. Trans. B 26B (1995) 361–382.
[10] R.C. Ruhl, Cooling rate in splat cooling, Mater. Sci. Engng. 1 (1967) 313–320.
[11] G.-X. Wang, E.F. Matthys, Modeling of heat transfer and solidification during splat cooling: effect of splat thickness and splat/substrate thermal contact, Int. J. Rapid Solidificat. 6 (1991) 141–174.
[12] G.-X. Wang, E.F. Matthys, On the heat transfer at the interface between a solidifying metal and a solid substrate, in: E.F. Matthys, W.G. Truckner (Eds.), Melt-Spinning, Strip Casting, and Slab Casting, TMS Publisher, Warrendale, PA, 1996, pp. 205–236.
[13] G.-X. Wang, E.F. Matthys, Experimental investigation of interfacial thermal resistance for molten metal solidification on a substrate, ASME J. Heat Transfer 118 (1996) 944–951.
[14] G.-X. Wang, Experimental and numerical study of heat transfer and solidification for molten metal in contact with a cold substrate, Ph.D. thesis, University of California, Santa Barbara, CA, 1995.
[15] G.-X. Wang, E.F. Matthys, Numerical modeling of phase change and heat transfer during rapid solidification processes: use of control volume integral with element subdivision, Int. J. Heat Mass Transfer 35 (1992) 141–153.
[16] J.C. Grosjean, J.L. Jacquot, J.M. Damasse, H. Litterscheidt, D. Senk, W. Schmitz, Thin strip casting experiments at Irsid and Thyssen Stahl AG, Iron & Steelmaker 20 (1993) 27–32.
[17] T.R. Thomas, in: Rough Surfaces, Longman, London, 1982, pp. 80–83.

[18] B.J. Keene, Review of data for the surface tension of pure metals, Int. Mater. Rev. 38 (1993) 157–192.
[19] E.A. Brandes, Smithells Metals Reference Book, sixth ed., Butterworths, London, 1983.
[20] Metals handbook, tenth ed., vol. 2, ASM Intl., Metal Park, OH, 1990, pp. 1110–1112; 1143.
[21] Metals handbook, tenth ed., vol. 1, ASM Intl., Metal Park, OH, 1990, pp. 195–199; 971.